Polyhedron 202 (2021) 115194

Contents lists available at ScienceDirect

Polyhedron

journal homepage: www.elsevier.com/locate/poly

Synthesis, characterization, crystal structures, Hirshfeld surface analysis, DFT computational studies and catalytic activity of novel oxovanadium and dioxomolybdenum complexes with ONO tridentate Schiff base ligand

Hadi Kargar [a,*], Maryam Bazrafshan [b], Mehdi Fallah-Mehrjardi [b], Reza Behjatmanesh-Ardakani [b], Hadi Amiri Rudbari [c], Khurram Shahzad Munawar [d,e], Muhammad Ashfaq [f], Muhammad Nawaz Tahir [f]

[a] Department of Chemical Engineering, Faculty of Engineering, Ardakan University, P.O. Box 184, Ardakan, Iran
[b] Department of Chemistry, Payame Noor University, 19395-3697 Tehran, Iran
[c] Department of Chemistry, University of Isfahan, Isfahan 81746-73441, Iran
[d] Department of Chemistry, University of Sargodha, Punjab, Pakistan
[e] Department of Chemistry, University of Mianwali, Mianwali, Pakistan
[f] Department of Physics, University of Sargodha, Punjab, Pakistan

ARTICLE INFO

Article history:
Received 2 February 2021
Accepted 30 March 2021
Available online 6 April 2021

Keywords:
Oxovanadium(V)
Dioxomolybdenum(VI)
Tridentate Schiff base
Homogeneous catalysis
Benzylic alcohols oxidation

ABSTRACT

For the first time, two new oxovanadium and dioxomolybdenum Schiff base complexes, **VOL(OMe)** and **MoO_2L**, were synthesized through the reaction of a ONO tridentate Schiff base ligand (**H_2L**) derived from the condensation of 5-bromosalicylaldehyde and nicotinic hydrazide with oxo and dioxo acetylacetonate salts of vanadium and molybdenum, [$VO(acac)_2$ and $MoO_2(acac)_2$], respectively. The synthesized ligand and complexes were characterized by various spectroscopic techniques like FT-IR, ^{1}H NMR, ^{13}C NMR, elemental analysis (CHN) and the most authentic single crystal X-ray diffraction analysis (SC-XRD). The geometry around the central metal ion in **MoO_2L** was distorted octahedral as revealed by the data collected from diffraction studies. Non-covalent interactions that are responsible for crystal packing are explored by Hirshfeld surface analysis. Theoretical calculations of the synthesized compounds, carried out by DFT at B3LYP/Def2-TZVP level of theory, indicated that the calculated results are in agreement with the experimental findings. Moreover, the catalytic activities of both complexes were investigated for the selective oxidation of benzylic alcohols using urea hydrogen peroxide (UHP) in acetonitrile.

1. Introduction

At present, it is necessary to look for the development of sustainable green technologies to be adopted in chemical synthesis to overcome energy crises. The use of revolutionary, innocuous and benign precursors and the employment of new catalytic systems with greater potency is the need of hour [1,2].

Aldehydes and ketones are considered as one of the most demanding reagents produced by the catalytic oxidation of benzyl alcohol (BzOH) [3]. This is because of extensive utilization of these carbonyls as precursors or intermediates in pharmaceutics, perfumes and vitamins [4]. The selective oxidation of BzOH is preferred to avoid generation of harmful and toxic by-products. This is generally carried out with the help of Cr(VI), I(VII), Mn(VII) and DMSO coupled with $(COCl)_2$ (Swern oxidation) [5,6]. These oxidizing agents are corrosive, expensive, toxic, difficult to handle, less selective and create serious environmental issues [7]. Moreover, by-products of Swern oxidation, methylthio methane, has not only the foul odor but also it is volatile, and the oxalyl chloride ($COCl_2$) is highly sensitive to humidity and its vapors are very toxic especially for respiratory systems [8,9].

In order to replace these traditional oxidants several transition metals complexes of iron, copper, cobalt, palladium, manganese [10–14], etc. have been outlined in literature. Moreover, oxovanadium(V) and dioxomolybdenum(VI) [15–19] complexes have been regarded as effective and valuable catalyst with high selectivity for the oxidation of BzOH in the presence of clean oxidants like molecular oxygen and hydrogen peroxide [20,21]. Molecular oxygen is considered as a perfect oxidant but it has poor selectivity and needs severe reaction conditions like elevated temperature and pressure. Hydrogen peroxide with 47% of oxygen contents may

* Corresponding author.
E-mail address: h.kargar@ardakan.ac.ir (H. Kargar).

https://doi.org/10.1016/j.poly.2021.115194
0277-5387/

be regarded as an appropriate oxidant due to its inexpensive nature, safe storage, good solubility and icing on cake, it generates water as a by-product [22–26]. But, the rate of oxidation reaction by hydrogen peroxide is very low due to its weak oxidizing capability and hence it is needed to be activated by using some suitable activating agents like sodium tungstate or hydrogen bromide [27,28]. So, instead of using highly unsafe liquid H_2O_2, the solid urea-hydrogen peroxide (UHP) in combination with oxovanadium(V) and dioxomolybdenum(VI) complexes is regarded as safer, greener and suitable substitute due to its easy availability, high stability and high hydrogen peroxide contents [29,30].

Hence, in culmination and continuation of our previous work [31], we are hereby reporting a novel and effective procedure for the selective oxidation of BzOH to aldehydes catalyzed by oxovanadium(V) and dioxomolybdenum(VI) complexes using urea hydrogen peroxide as oxidizing agent.

2. Experimental

2.1. Material and methods

All the chemicals employed in the current work were 99.9% pure and purchased from well renowned suppliers like Sigma-Aldrich and Merck. Elemental analysis was carried out by Heraeus CHN-O-FLASH EA 1112 instrument. ^{1}H and ^{13}C NMR spectra were measured at ambient temperature by using BRUKER AVANCE 400 MHz spectrometer in the presence of tetramethylsilane (TMS) as an internal standard. Coupling constant (J) and chemical shift (δ) values were reported in Hz and in ppm, respectively. Fourier transform infrared spectra of the synthesized compounds were taken, by making KBr pellets, with the help of IR Prestige-21 (Shimadzu).

2.2. Synthesis

2.2.1. Synthesis of ONO-tridentate Schiff base ligand (H_2L)

Nicotinic hydrazide (1.37 g, 10 mmol) and 5-bromosalicylaldehyde (2.01 g, 10 mmol) were dissolved separately in approximately 25 mL of hot methanol. After complete dissolution, both solutions were mixed dropwise with continuous stirring. The resulting mixture was refluxed for 3 h and the completion of reaction was ensured by ongoing monitoring with the help of TLC. On allowing the reaction mixture to attain the room temperature, the product was settled down leaving behind the impurities in the solvent. Finally, the desired product was collected by filtration, aided by suction apparatus and washed thrice with cold methanol to remove impurities if any. The prepared **H_2L** was finally crystalized from absolute ethanol to get the single crystal suitable for SC-XRD analysis.

H_2L: Yield 75%. *Anal.* Calc. for $C_{13}H_{10}BrN_3O_2$: C, 48.77; H, 3.15; N, 13.13, Found: C, 48.84; H, 3.19; N, 13.21%. FT-IR (KBr, cm^{-1}); 3269 (ν_{N-H}); 1678 ($\nu_{C=O}$); 1610 ($\nu_{C=N}$); 1591, 1477 ($\nu_{C=C}$); 1188 (ν_{C-O}); 1026 (ν_{N-N}). ^{1}H NMR (400 MHz DMSO d_6, ppm): 6.91 [1H, (H-*C*2), d, ^3J = 8.8 Hz], 7.44 [1H, (H-C3), dd, ^3J = 8.8 Hz, ^4J = 2.4 Hz], 7.58 [1H, (H-C12), dd, ^3J = 7.8 Hz, ^3J = 4.9 Hz], 7.82 [1H, (H-C5), d, ^4J = 2.4 Hz], 8.28 [1H, (H-C13), dd, ^3J = 6.5 Hz, ^4J = 1.7 Hz], 8.63 [1H, s, (CH = N)], 8.78 [1H, (H-C11), d,^3J = 3.9 Hz], 9.09 [1H, (H-C10) br], 11.18 [1H, s, (–NH)], 12.32 [1H, s, (–OH)]. ^{13}C NMR (100 MHz, DMSO d_6, ppm): 110.5 (*C*2), 118.7 (C6), 121.3 (C12), 123.6 (C4), 128.6 (C9), 130.2 (C5), 133.7 (C3), 135.5 (C13), 145.9 (C7), 148.6 (C10), 152.4 (C11), 156.4 (C1), 161.6 (C8).

2.2.2. Synthesis of VOL(OMe) complex

The new **VOL(OMe)** complex, where L = *(E)-N'*-(5-bromo-2-hydroxybenzylidene)nicotinohydrazide, was synthesized by treating [$V^{IV}O(acac)_2$] (1 mmol, 0.265 g, acac = acetylacetonate) with **H_2L** (1 mmol, 0.320 g) in methanol (50 mL). The mixture was kept under reflux for 3 h to obtain the solid product in the form of precipitates which were filtered off and then washed thoroughly with equal amounts of water, methanol and diethyl ether, separately.

VOL(OMe): Yield 61%. *Anal.* Calc. for $C_{14}H_{11}BrN_3O_4V$: C, 40.41; H, 2.66; N, 10.10, Found: C, 40.33; H, 2.69; N, 10.16%. FT-IR (KBr, cm^{-1}); 1614 ($\nu_{C=N}$); 1460 ($\nu_{C=N-N=C}$); 1286 (ν_{C-O}); 1029 (ν_{N-N}); 995 ($\nu_{V=O}$); 499 (ν_{V-O}); 476 (ν_{V-N}). ^{1}H NMR (400 MHz, DMSO d_6, ppm): 3.88 [3H, s, (–OCH_3)], 7.01 [1H, (H-*C*2), t, ^3J = 8.9 Hz], 7.55–7.59 [2H, (H-C12, H-C3), m], 7.88 [1H, (H-C5), d, ^4J = 2.7 Hz], 8.32 [1H, (H-C13), dt, ^3J = 8.0 Hz, ^4J = 1.8 Hz], 8.77 [1H, s, (CH = N)], 8.98 [1H, (H-C11), br], 9.15 [1H, (H-C10), br]. ^{13}C NMR (100 MHz, DMSO d_6, ppm): 66.3 (–OCH_3), 120.6 (C4), 121.5 (C), 124.0 (C6), 124.9 (C12), 125.9 (C9), 133.0 (C5), 134.4 (C3), 135.5 (C13), 148.8 (C10), 152.5 (C11), 155.7 (C1), 158.1 (C7), 167.7 (C8).

2.2.3. Synthesis of MoO_2L complex

Equimolar amounts of **H_2L** (1 mmol, 0.320 g) and [$Mo^{VI}O_2$(-acac)$_2$] (1 mmol, 0.330 g) were suspended in 100 mL of methanol in a round bottom flask equipped with a magnetic bar for steady stirring to attain the uniformity. The mixture was kept under reflux over a water bath for a period of 3 h until the solid product was precipitated out. The **MoO_2L** complex was then filtered off and washed meticulously with equal amounts of water, methanol and diethyl ether, separately, to remove impurities/by products if any. The precipitates were dried in *vacuo* and finally crystallized from CH_3CN to get orange-colored crystals.

MoO_2L: Yield 67%. *Anal.* Calc. for $C_{13}H_8BrMoN_3O_4$: C, 35.00; H, 1.81; N, 9.42, Found: C, 35.12; H, 1.87; N, 9.33%. FT-IR (KBr, cm^{-1}); 1616 ($\nu_{C=N}$); 1462 ($\nu_{C=N-N=C}$); 1265 (ν_{C-O}); 1018 (ν_{N-N}); 935 ($\nu_{O=Mo=O}$) *asym*; 914 ($\nu_{O=Mo=O}$) *sym*; 569 (ν_{Mo-O}); 480 (ν_{Mo-N}). ^{1}H NMR (400 MHz, DMSO d_6, ppm): 6.95 [1H, (H-*C*2), t, ^3J = 8.8 Hz], 7.57 [1H, (H-C12), dd, ^3J = 7.3 Hz, ^3J = 4.7 Hz], 7.68 [1H, (H-C3), dd, ^3J = 8.8 Hz, ^4J = 2.6 Hz], 8.00 [1H, (H-C5), d, ^4J = 2.6 Hz], 8.32 [1H, (H-C13), d, ^3J = 8.0 Hz], 8.78 [1H (H-C11), br], 8.98 [1H, s, (CH = N)], 9.16 [1H (H-C10), br]. ^{13}C NMR (100 MHz, DMSO d_6, ppm): 112.4 (*C*2), 120.9 (C6), 122.1 (C12), 124.0 (C4), 125.9 (C9), 135.5 (C5), 136.0 (C3), 137.2 (C13), 148.8 (C10), 152.5 (C11), 155.6 (C1), 158.5 (C7), 167.7 (C8).

2.3. X-ray crystallographic data collection H_2L ligand and MoO_2L complex

Single crystal X-ray studies of **H_2L** and **MoO_2L** were carried out on a STOE IPDS-II diffractometer by using Mo-Kα radiations monochromated by graphite. The data was collected at 298(2) K in a series of ω-scans in 1° oscillations and integrated by using the Stöe X-AREA [32] software package. A numerical absorption correction was applied using the X-RED [33] and X-SHAPE [34] software for the prepared compounds. The data was corrected for Lorentz and Polarizing effects. The structures were solved by direct methods using SIR2004 [35]. The non-hydrogen atoms were refined anisotropically by the full-matrix least-squares method on F^2 using SHELXL [36]. The collected crystallographic data of the ligand and its Mo complex are listed in Table S1.

2.4. Computational details

Density functional theory (DFT) calculations were performed with the Gaussian 09 package [37] at B3LYP level of theory [38] by using Def2-TZVP basis set [39]. The solution phase was modeled by using IEFPCM with the consideration of solvent (CH_3CN) [40]. Geometry optimizations were tested by frequency analysis to ensure that they are at the local minima on the molecular potential energy surface (PES). The results showed that there is

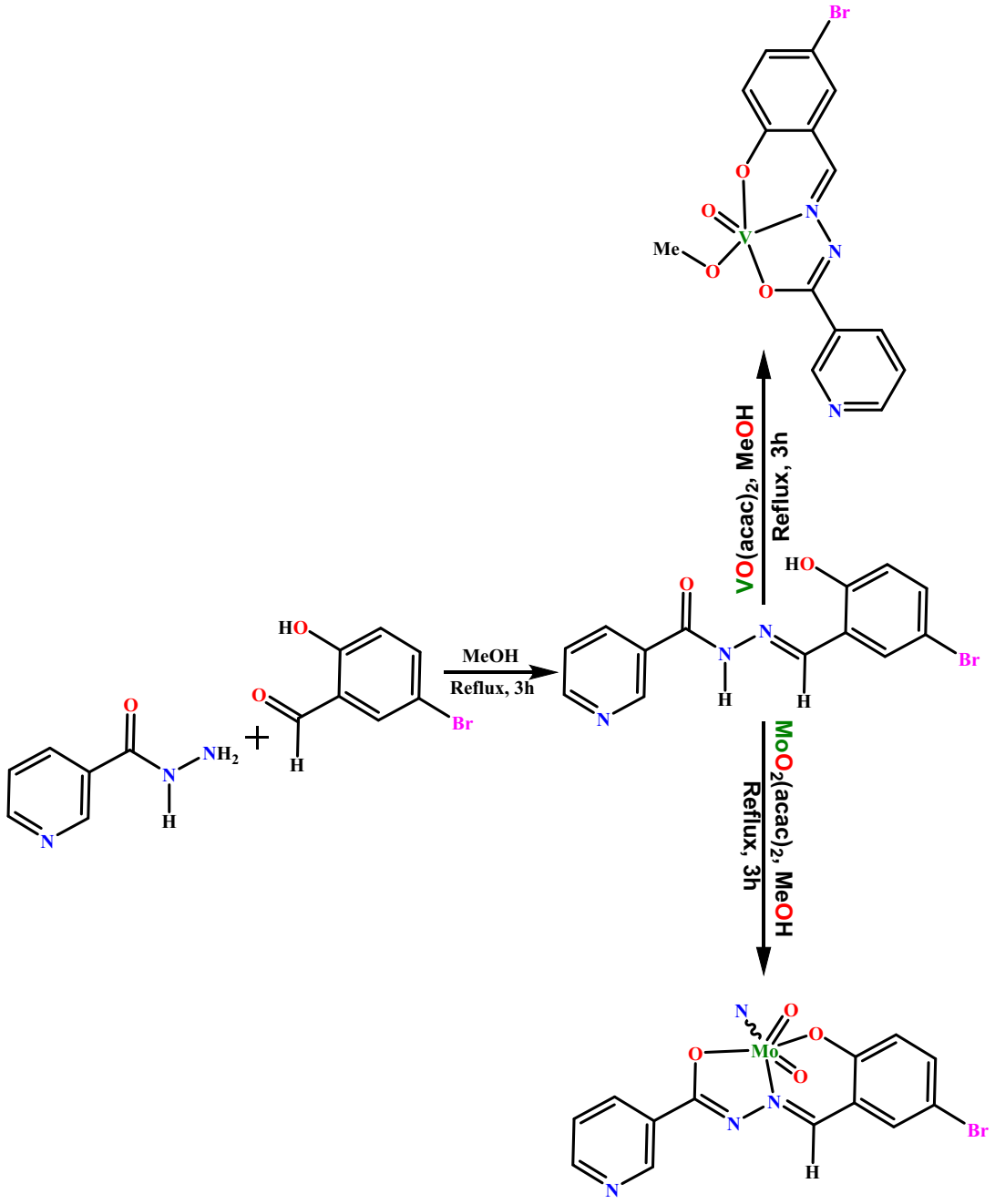

Scheme 1. Synthesis of H_2L Schiff base ligand and its respective VOL(OMe) and MoO_2L complexes.

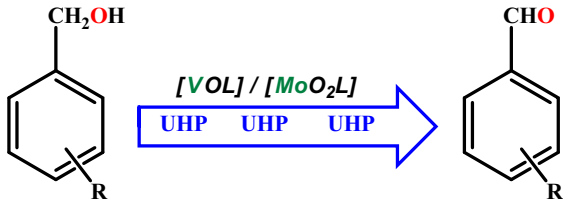

Scheme 2. Oxidation of benzylic alcohols using UHP carried out by homogeneous catalysts, VOL(OMe) and MoO_2L complexes.

no imaginary frequency. The ^1H and ^{13}C NMR magnetic isotropic shielding tensors were calculated by the standard Gauge-Independent Atomic Orbital (GIAO) approach in the solution phase [41–43]. Chemical shift values of compounds were calculated by using B3LYP/Def2-TZVP level and IEFPCM model as implicit model of solvent and compared with experimental data in DMSO d_6. The same solvent was used for all IEFPCM calculations for ligand, Mo complex and TMS. Chemical shifts were calculated by subtracting the appropriate isotropic part of the shielding tensor from that of TMS $\delta i = \sigma_{TMS} - \sigma i$. The isotropic magnetic shielding tensors for TMS calculated in the solution phase at the B3LYP/Def2-TZVP level of theory were equal to 31.92 and 184.52 ppm for the ^1H nuclei and the ^{13}C nuclei, respectively. The Chemissian program was used to draw contour plots of highest occupied molecular orbital (HOMO) and lowest unoccupied molecular orbital (LUMO) [44].

Table 1
The selected experimental and calculated bond lengths (Å) and angles (°) of H_2L ligand and MoO_2L complex.

Bond lengths	Experimental	Calculated	Bond Angles	Experimental	Calculated
H_2L Ligand					
C(7)–N(1)	1.262(7)	1.283	O(1)–C(1)–C(6)	122.8(5)	122.92
C(1)–O(1)	1.361(7)	1.332	C(1)–C(6)–C(7)	121.8(5)	122.09
N(1)–N(2)	1.382(7)	1.353	C(6)–C(7)–N(1)	118.6(5)	121.57
N(2)–C(8)	1.341(7)	1.382	C(7)–N(1)–N(2)	120.0(5)	118.97
C(8)–O(2)	1.231(7)	1.212	N(1)–N(2)–C(8)	117.6(5)	120.25
C(1)–C(6)	1.411(7)	1.416	N(2)–C(8)–O(2)	122.3(6)	122.67
Mo Complex					
Mo(1)–O(1)	1.935(4)	1.953	O(1)–Mo(1)–O(2)	149.16(14)	144.95
Mo(1)–O(2)	1.993(4)	2.016	O(1)–Mo(1)–O(3)	99.20(18)	100.00
Mo(1)–O(3)	1.677(4)	1.690	O(1)–Mo(1)–O(4)	103.71(18)	104.24
Mo(1)–O(4)	1.700(5)	1.698	O(2)–Mo(1)–O(3)	97.54(19)	99.48
Mo(1)–N(1)	2.246(4)	2.300	O(2)–Mo(1)–O(4)	96.35(17)	97.42
Mo(1)–N(3)	2.493(5)	2.598	O(3)–Mo(1)–O(4)	105.77(19)	107.14
N(1)–C(7)	1.289(7)	1.288	O(1)–Mo(1)–N(1)	82.02(18)	79.53
N(2)–C(8)	1.326(8)	1.302	O(2)–Mo(1)–N(1)	71.43(16)	70.32
N(1)–N(2)	1.384(7)	1.372	O(3)–Mo(1)–N(1)	92.88(19)	95.47
C(1)–O(1)	1.358(7)	1.332	O(4)–Mo(1)–N(1)	159.10(19)	141.28
C(8)–O(2)	1.313(8)	1.314	N(1)–Mo(1)–N(3)	80.58(17)	77.28

Table 2
Hydrogen-bond geometry (Å, °) for H_2L and MoO_2L.

Compounds	*D*—H···*A*	*D*—H	H···*A*	*D*···*A*	*D*—H···*A*
H_2L	O1—H1···N1	0.81 (7)	1.91 (7)	2.592 (7)	142 (7)
	N2—H2*A*···O1^{i}	0.86	2.26	3.121 (6)	176
	C5—H5···O2^{ii}	0.93	2.43	3.268 (7)	150
	C11—H11···N3^{iii}	0.93	2.56	3.439 (10)	158
MoO_2L	*C*2—H2···N2^{iv}	0.93	2.50	3.340 (9)	150
	C5—H5···O4^{v}	0.93	2.43	3.149 (8)	134

Symmetry codes: (i) $-x+1/2, y+1/2, z-1/2$; (ii) $-x+1/2, y+1/2, z+1/2$; (iii) $-x, -y+1, z-1/2$; (iv) $-x, y-1/2, -z+1/2$; (v) $-x, y+1/2, -z+1/2$

2.5. General procedure for the selective oxidation of benzylic alcohols catalyzed by VOL(OMe) and MoO_2L complexes

The **VOL(OMe)** or **MoO_2L** catalyst (0.006 mmol) was added to a solution of benzylic alcohol (1 mmol) and UHP (2 mmol) in CH_3CN (10 mL), and the reaction mixture was refluxed with continuous stirring for the specified intervals of times as listed in Table 9. The conversion of reactants into the products was observed continuously with the help of TLC plates by taking aliquots from reaction mixture. For this purpose, a mixture of *n*-hexane and ethyl acetate (7:3) was employed as an eluent. On complete conversion, the resultant mixture was filtered off and then the solvent was evaporated under reduced pressure. The corresponding benzaldehydes were finally obtained in pure form with the help of column chromatography using silica gel.

All products were known compounds, and also acknowledged by comparing their physicochemical characteristics, FT-IR and NMR spectra with those of authentic samples.

3. Results and discussion

3.1. Syntheses

A tridentate Schiff base ligand (**H_2L**) was prepared *via* reaction of equimolar amounts of nicotinic hydrazide with 5-bromosalicylaldehyde in methanolic medium. Reaction of $VO(acac)_2$ and $MoO_2(acac)_2$ with **H_2L** in the refluxed methanol, produces the targeted metal complexes (Scheme 1). After successful syntheses and characterization, the catalytic activity of the complexes was surveyed for the oxidation of various benzylic alcohols using UHP as a source of oxygen (Scheme 2).

3.2. Crystal structure determination

In **H_2L** (Figure S1, Table S1), 4-bromophenol ring A (C1-C6/O1/Br1), *N*′-methyleneformohydrazide moiety B (C7/C8/N1/N2/O2) and pyridine ring C (C9-C13/N3) are found to be planar with respective root mean square (r.m.s) deviation of 0.0034, 0.0266 and 0.0082 Å. *N*′-methyleneformohydrazide moiety B is orientated at dihedral angles of 7.7 (4)° and 28.8 (3)° with respect to rings A and C, respectively. Dihedral angle between ring A and C is 35.4 (2)°. The selected bond length and bond angles are stated in Table 1 and are found to be comparable to those observed in some closely related structures [45]. The molecular configuration is stabilized by intramolecular H-bonding of type N—H···O to form S (6) loop. The molecules are connected with each other through N—H···O bonding to form C7 zigzag chain that extends along $[1\bar{1}0]$ crystallographic direction as displayed in Figure S2a. The molecules are also interlinked by comparatively weak C—H···O, C—H···N, and C—H···Br bonding, displayed in Figure S2b. All the important parameters related to H-bonding geometry are specified in Table 2. In addition to hydrogen bonding, crystal packing is also stabilized by the presence of off-set π···π stacking interaction as displayed in Figure S3.

In **MoO_2L** (Fig. 1, Table S1) the coordination sphere around central Mo-atom comprises of two O-atoms and one *N*-atom from the chelating ligand, two O-atoms of oxo groups and one *N*-atom from pyridine ring of symmetry related molecule i) $1-x, -1/2+y, 1/2-z$. In the coordination sphere, equatorial sites are occupied by (N1/O1/O2/O4) atoms whereas, axial positions are engaged by (O3/N3^{i}) atoms. Bond lengths and bond angles in coordination sphere are such that a distorted octahedral geometry is formed. Selected bond lengths and bond angles are specified in Table 1. The Mo–O and Mo–N bond lengths in the complex are comparable

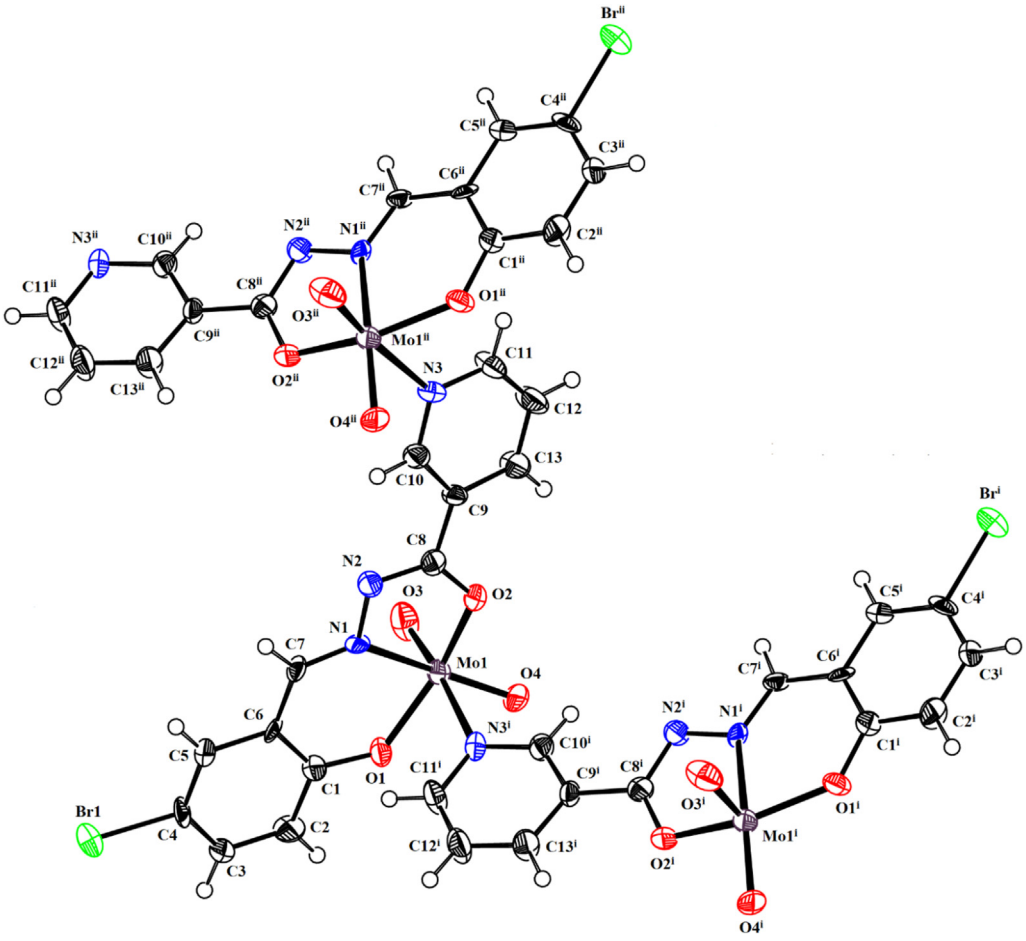

Fig. 1. ORTEP diagram representing polymeric form of MoO_2L. The Figure is drawn at probability level of 50% and H-atoms are displayed by small circles of arbitrary radii. i) $1 - x, -1/2 + y, 1/2 - z$, ii) $1 - x, 1/2 + y, 1/2 - z$.

to those observed in other oxomolybdenum complexes with hydrazone ligands [46]. In accordance with the previously reported bond lengths of the N1–N2 [1.1.385(6) Á] and the iminic N1–C7 [1.280(6) Á] groups were increased upon coordination to molybdenum center. The two Mo = O bond distances and the subtended O3-Mo1-O4 bond angle are comparable to the previously reported molybdenum complexes in literature [47]. The bromophenyl ring A (C1-C6/Br1) and pyridine ring B (C9-C13/N3) are found to be planar with respective r.m.s (root mean square) deviations of 0.0159 and 0.0091 Å with dihedral angle of 13.86 (4)° between ring A and B. Crystal structure is polymeric as shown in Fig. 4. Each polymeric chain is stabilized by C—H···O and C—H···N hydrogen bonding between molecules as displayed in Fig. 2 and specified in Table 2. Polymeric chains are interlinked by a weak interaction between aromatic rings known as off-set π...π stacking interaction. Bromo substituted phenyl ring of a molecule of a polymeric chain is found to be engaged with pyridine ring of another polymeric chain through off-set π...π stacking interaction with intercentroid separation of 3.757 Å and ring off-set value of 1.298 Å as shown in Fig. 3.

3.3. Optimized structural parameters

To determine and analyze the exact structures of the ligand and its complexes, DFT method at the B3LYP/Def2-TZVP level of theory in the gas phase was used. The optimized structures of compounds are shown in Fig. 4 and the selected experimental and calculated bond lengths and bond angles of the **H_2L** ligand and **MoO_2L** complex are listed in Tables 1. As shown in Table 1, the theoretical and experimental results are comparable. The differences between the theoretical and experimental values may emanate from this fact that the experimental data belong to the solid state, while the calculated values describe a single molecule in the gaseous state. In accordance with X-ray crystal structures, the coordination of nitrogen and oxygen atoms to the metal center of Mo complex in the gas phase exhibit the distorted octahedral geometry.

3.4. FT-IR spectra

The FT-IR spectra of the **H_2L** ligand and its oxovanadium and dioxomolybdenum complexes are presented in Figure S4. A careful comparison of the FT-IR spectra of the synthesized compounds was carried out to look deeply into the sites of coordination of ligands to metals. The FT-IR spectrum of the ligand showed two bands in the region of 3269 and 1678 cm^{-1} which correspond to the stretching vibrations of the ν(NH) and ν(C=O). These bands disappear in the spectra of the complexes which is in accordance with the enolization of the amide functional group, followed by deprotonation to attach with metal ions. The X-ray diffraction data also confirm the same mode of coordination of the ligand. The particular stretching vibration of azomethine group (–HC = N) in ligand appeared at 1610 cm^{-1} also showed a slight shift on complexation. New bands emerging at 1265 and 1286 cm^{-1} are attributed to enolic ν(C—O) moiety in molybdenum and vanadium complexes, respectively. In addition, the appearance of two new bands at 914 and 935 cm^{-1} are assigned

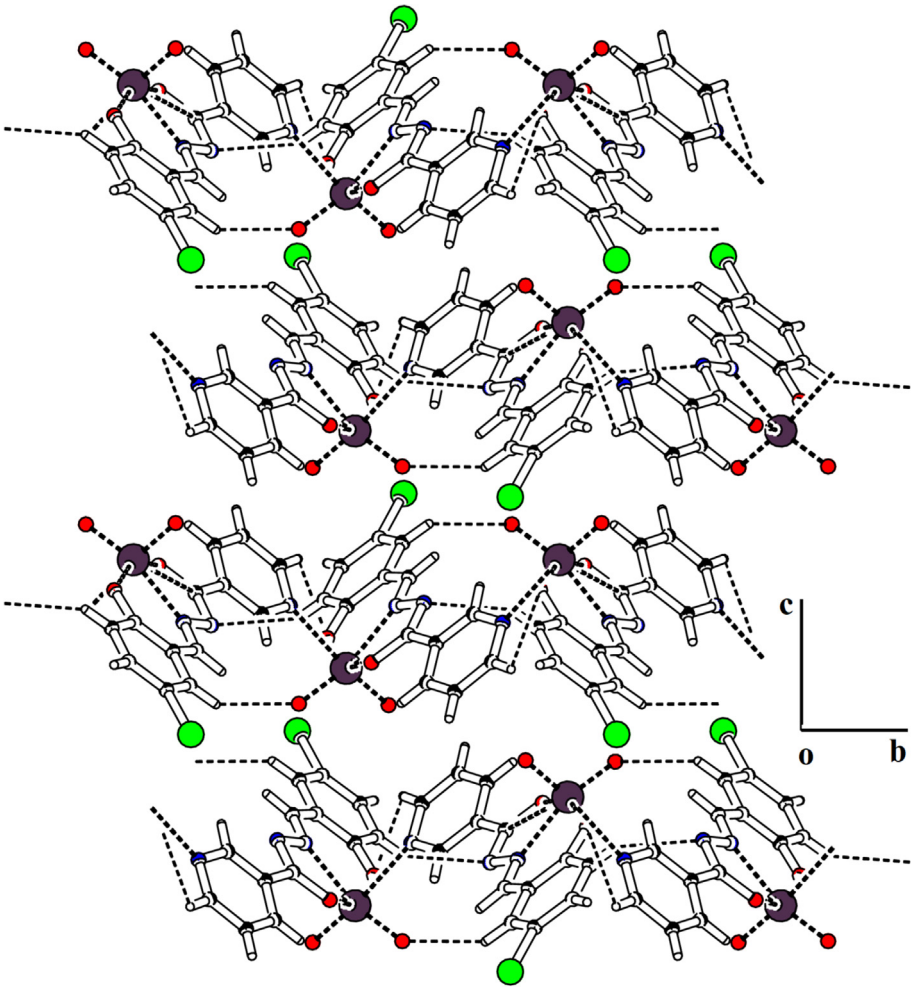

Fig. 2. Packing diagram of MoO_2L indicating that polymeric chains are stabilized by hydrogen bonding.

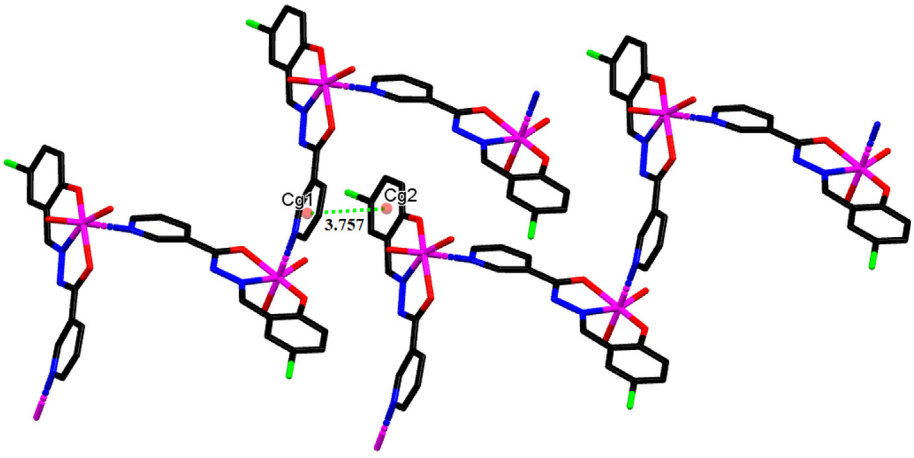

Fig. 3. Graphical representation of off-set π…π interaction for MoO_2L. Distance is measured in Å and H-atoms are omitted for the sake of clarity.

to symmetric and asymmetric stretching vibrations of the *cis*-MoO_2 moiety which are in accordance with similar structures reported previously in the literature [48,49]. Similarly, oxovanadium complex also gives its characteristics peak of V = O at 995 cm^{-1} which is very close to the values for the similar oxovanadium Schiff base complexes already reported in the literature [48–50]. Moreover, some new M–O and M–N peaks are also visible at 569 and 480 cm^{-1} for Mo complex and at 499 and 476 cm^{-1} for V complex, respectively, which are also in agreement to the similar complexes reported earlier [51–54].

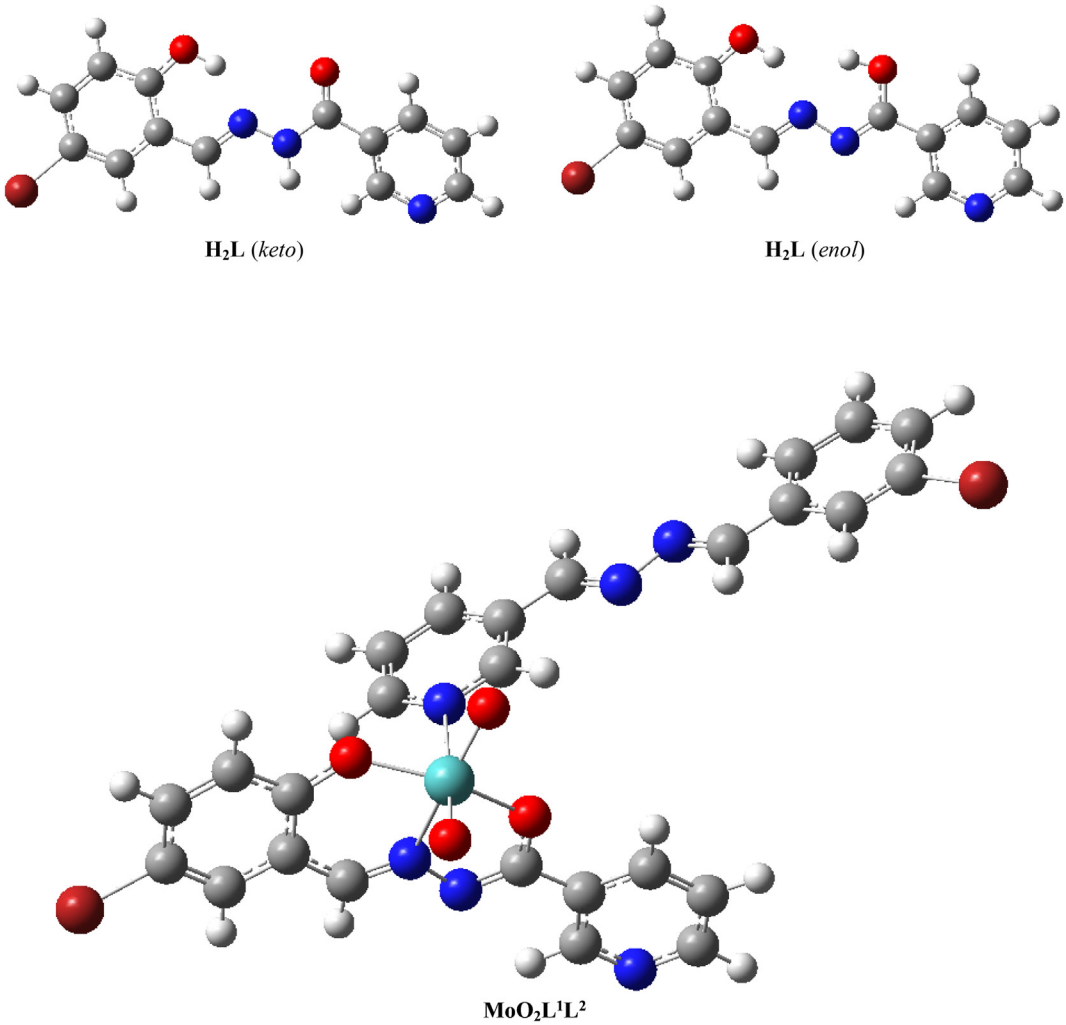

Fig. 4. Optimized structures of H_2L ligand (*keto* and *enol* forms) and $MoO_2L^1L^2$ complex.

Table 3
Selected experimental and calculated FT-IR frequencies of the H_2L ligand and MoO_2L complex (cm^{-1}).

Assignment	H_2L			MoO_2L		
	Exp.	Calc.	Relative error (%)	Exp.	Calc.	Relative error (%)
C=N	1610	1551	−3.66	1616	1660	2.72
C—O	1188	1270	6.90	1265	1296	2.45
M−O	–	–	–	569	606	6.50
M−N	–	–	–	480	479	−0.21

Table 4
Experimental and calculated ^1H and ^{13}C NMR shifts of H_2L ligand and MoO_2L complex (ppm).

Protons	^1H NMR				Carbons	^{13}C NMR			
	H_2L		MoO_2L			H_2L		MoO_2L	
	Exp.	Calc.	Exp.	Calc.		Exp.	Calc.	Exp.	Calc.
OH	12.32	11.85	–	–	C8	161.6	169.6	167.7	175.8
NH	11.18	9.23	–	–	C1	156.4	168.7	155.6	167.8
CH(10)	9.09	9.29	9.16	9.83	C11	152.4	161.5	152.5	161.1
CH(11)	8.78	9.15	8.78	9.09	C10	148.6	154.4	148.8	158.7
HC = N	8.63	8.43	8.98	9.18	C7	145.9	154.5	158.5	167.5
CH(13)	8.28	8.65	8.32	8.56	C13	135.5	144.7	137.2	143.6
CH(5)	7.82	7.66	8.00	7.95	C3	133.7	142.3	136.0	148.4
CH(12)	7.58	7.82	7.57	7.76	C5	130.2	141.3	135.5	145.1
CH(3)	7.44	7.67	7.68	7.95	C9	128.6	136.9	125.9	131.9
CH(2)	6.91	7.27	6.95	7.25	C4	123.6	135.4	124.0	139.9
					C12	121.3	130.6	122.1	130.0
					C6	118.7	126.5	120.9	127.2
					C2	110.5	124.1	112.4	126.1

Table 5
The Mulliken atomic charges of the H_2L ligand and MoO_2L complex.

Atoms	H_2L	MoO_2L	Atoms	H_2L	MoO_2L
M1	–	1.609	C3	−0.125	−0.126
Br1	−0.095	−0.069	C4	0.089	0.102
O1	−0.377	−0.566	C5	−0.237	−0.255
O2	−0.327	−0.541	C6	0.102	0.041
O3	–	−0.536	C7	−0.017	0.047
O4	–	−0.545	C8	0.286	0.445
N1	−0.165	−0.248	C9	0.055	0.011
N2	−0.169	−0.166	C10	−0.101	−0.069
N3	−0.208	−0.201	C11	−0.026	−0.020
C1	0.200	0.400	C12	−0.082	−0.093
C2	−0.197	−0.186	C13	−0.150	−0.138

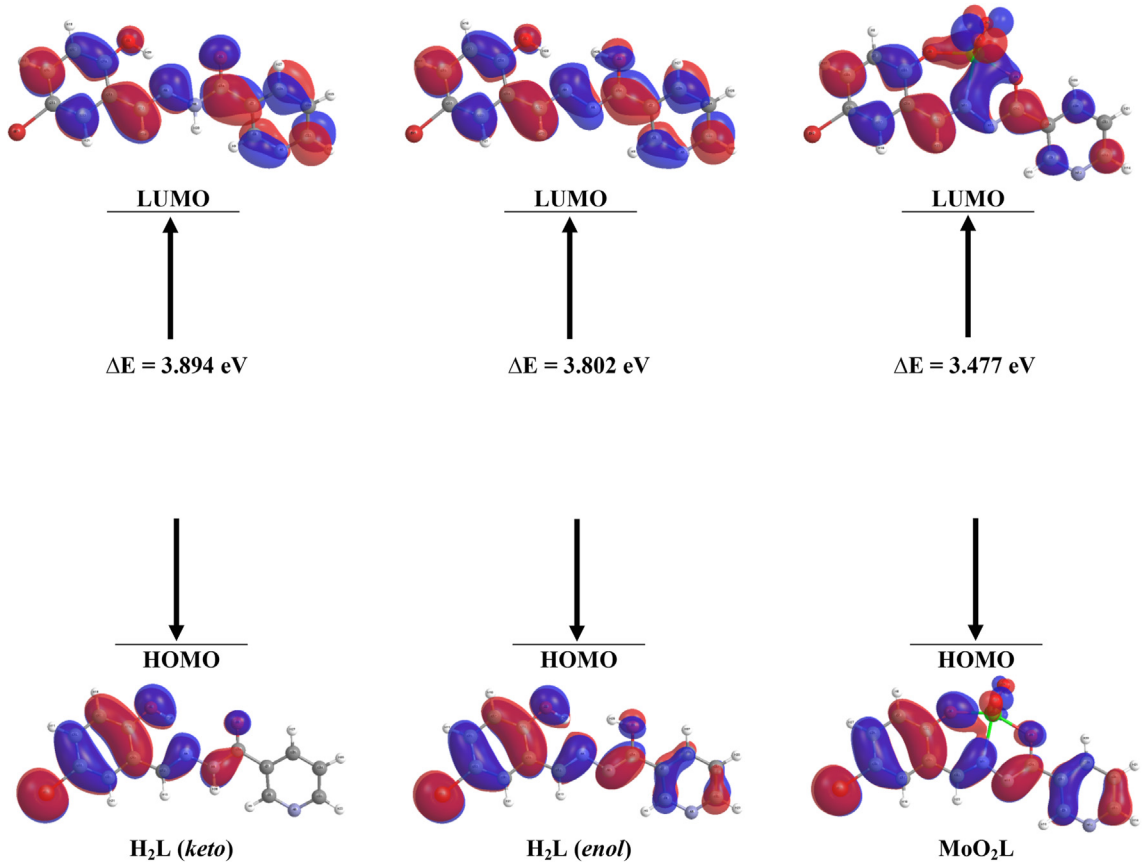

Fig. 5. DFT-optimized frontier molecular orbitals for H_2L ligand (*keto* and *enol*) and MoO_2L complex.

Table 6
The HOMO and LUMO energies and the energy gaps of the H_2L ligand and MoO_2L complex.

E (eV)	H_2L (*keto*)	H_2L (*enol*)	MoO_2L
E_{HOMO}	−6.282	−6.377	−6.847
E_{LUMO}	−2.388	−2.575	−3.397
*Energy gap	3.894	3.802	3.477

*Eg = E_{LUMO} - E_{HOMO}

Selected experimental and theoretical vibrational modes of the **H_2L** ligand and **MoO_2L** complex are listed in Table 3, which shows that there is a good correlation between theoretical data and experimental results.

3.5. ^1H and ^{13}C NMR spectra

The ^1H and ^{13}C NMR spectra of **H_2L**, **VOL(OMe)** and **MoO_2L** recorded in DMSO d_6 are presented in the experimental section and also shown in Figures S5-S10. Two signals appearing at δ = 12.32 and 11.18 ppm in the ^1H NMR spectrum of the ligand correspond to OH (phenolic) and NH protons, respectively, disappear on treatment with V and Mo salts, demonstrating that the sites of coordination are phenolate and enolate oxygens of the ligand with the metals. This also ascertains the occurrence of keto-imine tautomerism upon complexation. Moreover, a singlet signal of azomethine proton (–HC = N) at δ = 8.63 ppm observed in the spectra of the ligand was shifted downfield at δ = 8.77 in **VOL(OMe)** and δ = 8.98 ppm in **MoO_2L** showing the deshielding due to the decrease in the electronic density upon the coordination of azomethine nitrogen with the metal center. This is in accordance with the FT-IR spectra of the complex, where ν(HC = N) appears at higher

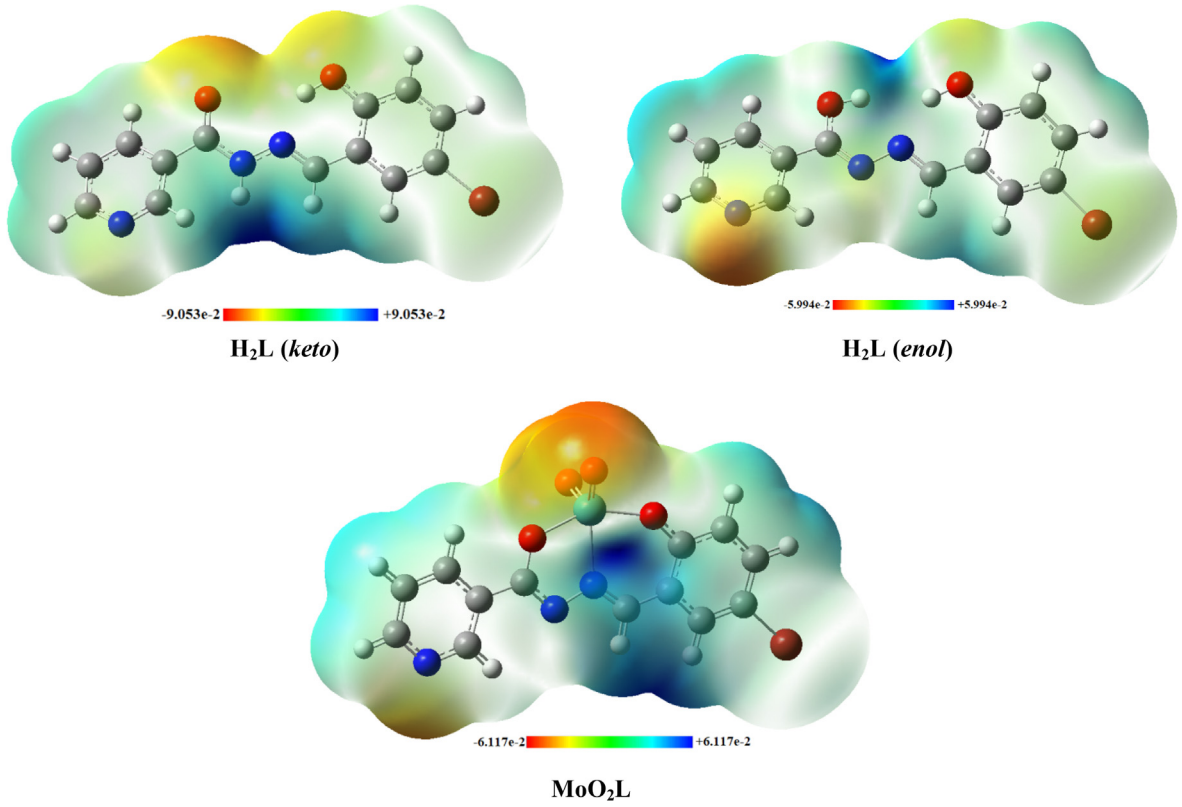

Fig. 6. Molecular electrostatic potential (MEP) for H_2L ligand (*keto* and *enol*) and MoO_2L complex with color range along with scale.

Table 7
Sum of the electronic and the zero-point energy (E^{ZPE}), enthalpy (H), and Gibbs free energy (G) of the ligand. All values are in Hartree unit.

	H_2L (*keto*) Gas phase	Solution phase	H_2L (*enol*) Gas phase	Solution phase
E^{ZPE}	−3390.373	−3390.390	−3390.365	−3390.376
H	−3390.355	−3390.366	−3390.348	−3390.353
G	−3390.420	−3390.449	−3390.412	−3390.437

1 Hartree = 627.5095 kcal.mol^{-1}

Table 8
Effect of the solvent, temperature, oxidant and catalyst amount for the oxidation of 4-chlorobenzyl alcohol catalyzed by **VOL(OMe)** and **MoO_2L** complexes[a].

Entry	Oxidant	Catalyst (mmol)	Solvent	Condition	VOL(OMe)		MoO_2L	
					Time (min)	Yield (%)	Time (h)	Yield (%)
1	UHP	0.006	EtOH	Reflux	10	50	2	37
2	UHP	0.006	Acetone	Reflux	10	78	2	55
3	UHP	0.006	MeOH	Reflux	10	68	2	53
4	**UHP**	**0.006**	**MeCN**	**Reflux**	**10**	**92**	**2**	**90**
5	UHP	0.006	DCE	Reflux	10	33	2	20
6	UHP	0.006	$CHCl_3$	Reflux	10	30	2	22
7	UHP	0.006	CCl_4	Reflux	10	15	2	5
8	UHP	0.006	CH_2Cl_2	Reflux	10	5	2	Trace
9	UHP	0.006	MeCN	r.t.	10	Trace	2	Trace
10	UHP	0.006	MeCN	50 °C	10	50	2	45
11	UHP	0.006	MeCN	70 °C	10	82	2	81
12	No oxidant	0.006	MeCN	Reflux	10	0	2	0
13	$NaIO_4$	0.006	MeCN	Reflux	10	20	2	25
14	H_2O_2	0.006	MeCN	Reflux	10	40	2	50
15	$(Bu)_4NIO_4$	0.006	MeCN	Reflux	10	10	2	10
16	TBHP	0.006	MeCN	Reflux	10	60	2	50
17	UHP	0	MeCN	Reflux	10	0	2	0
18	UHP	0.002	MeCN	Reflux	10	45	2	40
19	UHP	0.004	MeCN	Reflux	10	68	2	65
20	UHP	0.008	MeCN	Reflux	10	92	2	91

[a] Reaction conditions: 4-chlorobenzyl alcohol (1 mmol), oxidant (2 mmol), catalyst, solvent (10 mL) under different temperatures

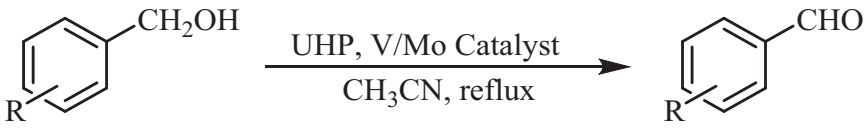

Scheme 3. Selective oxidation of benzyl alcohols by oxo-V(V) and dioxo-Mo(VI) complexes.

Table 9
Selective oxidation of benzylic alcohols to benzaldehydes with UHP catalyzed by VOL(OMe) and MoO_2L complexes[a].

Entry	Alcohol	Aldehyde[b]	VOL(OMe)		MoO_2L	
			Time (min)	Yield (%)[c]	Time (h)	Yield (%)[c]
1	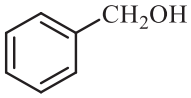	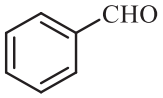	10	94	2	91
2	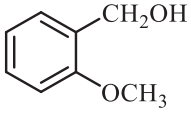	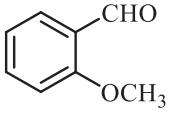	20	93	2.5	90
3	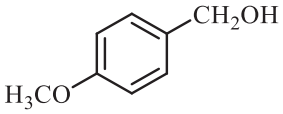	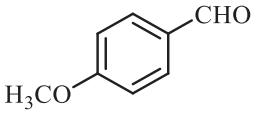	10	92	2	89
4	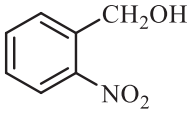	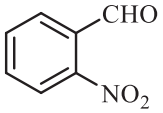	15	88	2.5	91
5	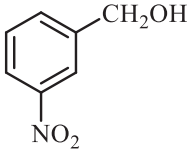	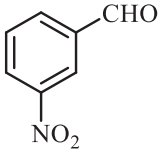	20	91	2.5	89
6	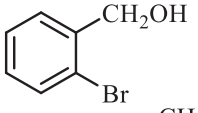	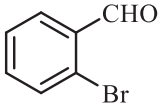	10	92	2	90
7	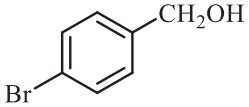	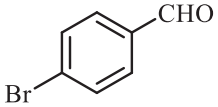	15	93	2.5	91
8	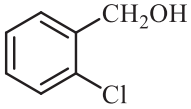	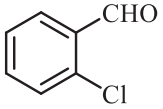	10	90	2	89
9	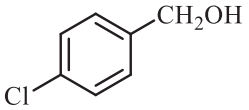	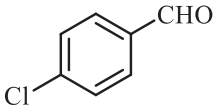	10	92	2	90
10	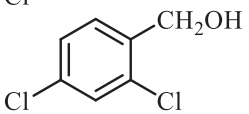	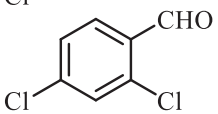	20	94	3	90

[a] Reaction conditions: benzylic alcohol (1 mmol), UHP (2 mmol), catalyst (0.006 mmol), CH_3CN (10 mL) under reflux conditions
[b] All products were identified by comparison of their physical and spectral data with those of authentic samples
[c] Isolated Yield

wavenumber in comparison with the corresponding free ligand. All the signals of aromatic protons in the ^1H NMR spectrum of the ligand were observed in the expected range of δ = 6.91–9.09 ppm. There is a slight shift in the positions of signals of aromatic protons of the ligand upon complex formation (δ = 7.01–9.15 ppm in **VOL(OMe)** and δ = 6.95–9.16 ppm in **MoO_2L**).

The ^{13}C NMR spectra of the ligand and its V and Mo complex are shown in Figures S8-S10. The signals for the carbonyl, phenolic and methine carbon in the V complex were observed at δ = 167.7, 158.1 and 155.7 ppm, respectively and in the Mo complex were observed at δ = 167.7, 158.5 and 155.6 ppm, respectively. The chemical shift values of the carbons present in vicinity of the coordinating atoms (i.e. C8, C1 and C7) showed appreciable change in their position due to coordination-induced shifts confirming the association of these functionalities in coordination. The other aromatic carbons of ligand and its complexes appeared in their respective regions according to the literature [55]. The experimental and calculated ^1H and ^{13}C NMR chemical shifts of the ligand and its Mo complex

are given in Table 4. It is obvious from the table that the theoretical data are in agreement with the experimental findings.

3.6. Mulliken atomic charges distribution

From Mulliken charge data of **H_2L** ligand and its dioxomolybdenum complex (Table 5) it can be seen that the Mulliken charge at the central atom is + 1.609e in Mo complex. The metal atom charge is considerably lower than formal charge 6 + for molybdenum, which indicates that the significant amount of charge density is transferred from the ligand to the metal atom. Also, the highest charge density in the ligand was found on C1 and C8 atoms, which increases, from 0.200 to 0.400 for C1, and from 0.286 to 0.445 for C8, in the gas phase, after the complexation with molybdenum.

3.7. Electronic properties

The frontier highest occupied molecular orbital (HOMO) and the lowest unoccupied molecular orbital (LUMO) are the most necessary orbitals to describe the chemical activity of the compounds. To obtain the electronic distribution of frontier orbitals, the HOMO and LUMO energy levels of the ligand and its Mo complex, were computed by B3LYP/Def2-TZVP level of theory. The results are presented in Fig. 5. The HOMO and LUMO energies for the compounds and their energy gaps (ΔE) are listed in Table 6. The energy gaps for the **H_2L** (keto), **H_2L** (enol) and **MoO_2L** were found to be 3.894, 3.802 and 3.477 eV, respectively. The energy gap of **H_2L** (keto) is slightly greater than that of **H_2L** (enol), which can be attributed to higher stability of keto tautomeric form of the ligand.

Molecular electrostatic potential (MEP) can be used for the recognition of the chemical activity of the molecules and to look for the relationship of molecular structures with physicochemical properties. The MEP can display electrophilic sites (positive regions) and nucleophilic sites (negative regions) of the molecule based on their electrostatic potentials, which are represented by blue and red colors, respectively. The MEP diagrams and values of electrostatic potentials of **H_2L** ligand and **MoO_2L** complex are presented in Fig. 6. There is a significant difference between electrostatic potential values of enol and keto forms of **H_2L** ligand. In keto form, the more negative site is located between the oxygen atoms of phenolic and carbonyl groups, with electrostatic value of $\sim$ 57 kcal.mol^{-1}, while in enol form, the blue color can be observed between two hydroxyl groups which means this area has electrophilic property and has positive electrostatic potential ($\sim$38 kcal.mol^{-1}). In the dioxomolybdenum complex with electrostatic potential value of $\sim$ 38 kcal.mol^{-1}, the metal atom is the center of positive potential represented by blue color which means it is a good candidate for attack by a nucleophile. These results are consistent with the Mulliken atomic charges (Table 5).

The sum of the electronic and the zero-point energy (E^{ZPE}), enthalpy (H), and Gibbs free energy (G) of both enol and keto forms of **H_2L** Schiff base ligand are reported in Table 7. Data showed that keto form is more stable in both gas and solution phases. This is in agreement with the results from the molecular electrostatic potential (MEP) values and from the comparison of energy gaps between HOMO and LUMO of keto and enol tautomeric forms of the ligand (See Figures 17 and 18).

3.8. Catalytic activity studies

Oxovanadium and dioxomolybdenum complexes have attracted particular attention as prominent catalysts, especially in oxidation reactions [56,57]. Compared to the reported species, the present two complexes have excellent efficiency. The catalytic activity of **VOL(OMe)** and **MoO_2L** complexes was studied for the selective oxidation of benzylic alcohols to the corresponding benzaldehydes under various reaction conditions.

In order to optimize the conditions, the oxidation of 4-chlorobenzyl alcohol (1 mmol) using UHP (2 mmol) was chosen as a model reaction, and the influence of different factors, that may affect the reaction, were investigated (Table 8). First, various solvents like acetonitrile, acetone, methanol, ethanol, 1,2-dichloroethane (DCE), chloroform, carbon tetrachloride and dichloromethane were tested in the presence of UHP as oxidant, and oxovanadium or dioxomolybdenum complexes as the catalyst. The results showed that the use of acetonitrile imparts a higher yield of 4-chlorobenzaldehyde both for V and Mo complexes (Entries 1–8).

By changing the reaction temperature, the catalytic oxidation reaction of 4-chlorobenzyl alcohol with UHP in the presence of V or Mo complexes in CH_3CN was performed (Entries 4, 9–11). It can be found that the rate of reaction increases with the increase of temperature, resulting in the enhancement of 4-chlorobenzaldehyde yield in the same period of time. For all kinds of substrates, the best yield was observed under reflux conditions which requires 10 min. for **VOL(OMe)** complex and 2 h for **MoO_2L** complex to complete the reaction.

The effect of different oxidants (2 mmol) including $NaIO_4$, H_2O_2, urea H_2O_2 (UHP), Bu_4NIO_4 and *tert*-BuOOH (TBHP) was also investigated and the results showed that UHP is the best oxygen source in this reaction (Entries 4, 12–16).

Different amounts of the catalysts were used (Entries 4, 17–20) and it was observed that in the absence of the catalyst the reaction failed to proceed. The rate of conversion was increased with the increase in the amount of catalyst and complete transformation was cropped up when 0.006 mmol of the catalyst was used.

The generality of this procedure for the oxidation of various substituted benzylic alcohols was demonstrated in the presence of **VOL(OMe)** and **MoO_2L** complexes as homogeneous catalysis under the optimal conditions (Scheme 3, Table 9). As shown in Table 9, a variety of benzylic alcohols, with both electron-donating and electron-withdrawing groups, are treated with UHP to give the corresponding substituted benzaldehydes in excellent yields.

The chemoselectivity of the procedure was remarkable. The benzylic hydroxyl groups were oxidized under the affection of this catalytic system and the desired benzaldehydes were obtained in 100% selectivity. The most important advantage of this method is that there is no evidence of overoxidation to the production of carboxylic acid in all the studied substrates.

4. Conclusion

In this research, we synthesized a new tridentate ONO-donor Schiff base ligand and its V(V) and Mo(VI) complexes and characterized them by various physicochemical techniques. The molecular structures of ligand and dioxomolybdenum complex were determined by single crystal X-ray crystallography. The coordination geometry around Mo metal center was found to be distorted octahedral. Non-covalent interactions are explored by Hirshfeld surface analysis. Theoretical calculations of the Schiff base ligand and its Mo complex were performed using DFT at B3LYP/Def2-TZVP level of theory. The results showed that theoretical data is in good consensus with the experimental outcomes. The catalytic activities of the complexes were also investigated for the selective oxidation of benzylic alcohols to benzaldehydes by the use of UHP in acetonitrile under reflux conditions. This method has numerous ascendancies such as high yield, short reaction time and excellent selectivity to produce corresponding benzaldehydes without overoxidation to carboxylic acids.

Declaration of Competing Interest

The authors declare that they have no known competing financial interests or personal relationships that could have appeared to influence the work reported in this paper.

Acknowledgements

We gratefully acknowledge the practical support of this study by Ardakan University and Payame Noor University.

Appendix A. Supplementary data

Supplementary data to this article can be found online at https://doi.org/10.1016/j.poly.2021.115194.

References

[1] G. Chen, Y.u. Zhou, Z. Long, X. Wang, J. Li, J. Wang, Mesoporous polyoxometalate-based ionic hybrid as a triphasic catalyst for oxidation of benzyl alcohol with H_2O_2 on water, ACS Appl. Mater. Interfaces 6 (6) (2014) 4438–4446.
[2] P.T. Anastas, J.C. Warner, Principles of green chemistry, Green Chemistry: Theory and Practice, Oxford University Press, Oxford, UK, 1998.
[3] M.Á. Gaona, F. Montilla, E. Álvarez, A. Galindo, Synthesis, characterization and structure of nickel and copper compounds containing ligands derived from keto-enehydrazines and their catalytic application for aerobic oxidation of alcohols, Dalton Trans. 44 (14) (2015) 6516–6525.
[4] S. He, X. Chen, F. Zeng, P. Lu, Y. Peng, L. Qu, B. Yu, Visible-light-promoted oxidative decarboxylation of arylacetic acids in air: Metal-free synthesis of aldehydes and ketones at room temperature, Chin. Chem. Lett. 31 (2020) 1863–1867.
[5] R.A. Sheldon, I.W.C.E. Arends, A. Dijksman, New developments in catalytic alcohol oxidations for fine chemicals synthesis, Catal. Today 57 (1-2) (2000) 157–166.
[6] D.G. Lee, U.A. Spitzer, Aqueous dichromate oxidation of primary alcohols, J. Org. Chem. 35 (10) (1970) 3589–3590.
[7] F. Gaspar, C.D. Nunes, Selective catalytic oxidation of benzyl alcohol by MoO_2 Nanoparticles, Catalysts 10 (2020) 265–279.
[8] S.C.A. Sousa, J.R. Bernardo, A.C. Fernandes, Highly efficient oxidation of benzyl alcohols using the catalytic system sulfoxide/oxo-complexes, Tetrahedron Lett. 53 (46) (2012) 6205–6208.
[9] L. De Luca, G. Giacomelli, A. Porcheddu, J. Org. Chem. 66 (2001) 7907–7909.
[10] R.R. Fernandes, J. Lasri, M.F.C. Guedes da Silva, J.A.L. da Silva, J.J.R. Frausto da Silva, A.J.L. Pombeiro, Appl. Catal. A 402 (2011) 110–120.
[11] J.U. Ahmad, M.T. Räisänen, M. Leskelä, T. Repo, Copper catalyzed oxidation of benzylic alcohols in water with H_2O_2, Appl. Catal. A 411-412 (2012) 180–187.
[12] K. Kervinen, H. Korpi, M. Leskelä, T. Repo, Oxidation of veratryl alcohol by molecular oxygen in aqueous solution catalyzed by cobalt salen-type complexes: the effect of reaction conditions, J. Mol. Catal. A: Chem. 203 (1-2) (2003) 9–19.
[13] M.N. Missaghi, J.M. Galloway, H.H. Kung, Bis(pyridyl)siloxane-Pd(II) complex catalyzed oxidation of alcohol to aldehyde: Effect of ligand tethering on catalytic activity and deactivation behavior, Appl. Catal. A 391 (2011) 297–304.
[14] M.M. Najafpour, M. Amini, M. Bagherzadeh, D.M. Boghaei, V. McKee, Synthesis, structural characterization and alcohol oxidation activity of a new mononuclear manganese(II) complex, Transition Met. Chem. 35 (3) (2010) 297–303.
[15] K. Alagiri, K.R. Prabhu, Efficient synthesis of carbonyl compounds: oxidation of azides and alcohols catalyzed by vanadium pentoxide in water using tert-butylhydroperoxide, Tetrahedron 67 (2011) 8544–8551.
[16] J.A.L. da Silva, J.J.R.F. da Silva, A.J.L. Pombeiro, Oxovanadium complexes in catalytic oxidations, Coord. Chem. Rev. 255 (19-20) (2011) 2232–2248.
[17] A.V. Biradar, M.K. Dongare, S.B. Umbarkar, Selective oxidation of primary aromatic alcohols to aldehydes using molybdenum acetylide oxo-peroxo complex as catalyst, Tetrahedron Lett. 50 (2009) 2885–2888.
[18] S. Velusamy, M. Ahamed, T. Punniyamurthy, Novel polyaniline-supported molybdenum-catalyzed aerobic oxidation of alcohols to aldehydes and ketones, Org. Lett. 6 (26) (2004) 4821–4824.
[19] K. Jeyakumar, D.K. Chand, Aerobic oxidation of benzyl alcohols by MoVI compounds, Appl. Organomet. Chem. 20 (12) (2006) 840–844.
[20] N. Noshiranzadeh, M. Mayeli, R. Bikas, K. Ślepokura, T. Lis, Selective catalytic oxidation of benzyl alcohol to benzaldehyde by a mononuclear oxovanadium (V) complex of a bis (phenolate) ligand containing bulky tert-butyl substituents, Transition Met. Chem. 39 (2014) 33–39.
[21] S. Parihar, R.N. Jadeja, V.K. Gupta, Novel oxovanadium (IV) complexes with 4-acyl pyrazolone ligands: synthesis, crystal structure and catalytic activity towards the oxidation of benzylic alcohols, RSC Adv. 4 (2014) 295–302.
[22] J.S. Carey, D. Laffan, C. Thomson, M.T. Williams, Analysis of the reactions used for the preparation of drug candidate molecules, Org. Biomol. Chem. 4 (12) (2006) 2337, https://doi.org/10.1039/b602413k.
[23] C. Parmeggiani, F. Cardona, Transition metal based catalysts in the aerobic oxidation of alcohols, Green Chem. 14 (3) (2012) 547, https://doi.org/10.1039/c2gc16344f.
[24] A. Goti, F. Cardona, Hydrogen peroxide in green oxidation reactions: Recent catalytic processes, Berlin/Heidelberg, Germany, In Green Chemical Reactions; Springer, 2008.
[25] C. Jones, Applications of hydrogen peroxide and derivatives, Royal Society of Chemistry, Cambridge, UK, 1999.
[26] G. Strukul, Catalytic oxidations with hydrogen peroxide as oxidant, Kluwer Academic, Dordrecht, Netherlands, 1992.
[27] B.S. Chhikara, R. Chandra, V. Tandon, A versatile method for the hydrogen peroxide oxidation of alcohols using PTC condition in tert-butanol, Synlett 36 (33) (2005), https://doi.org/10.1002/(ISSN)1522-266710.1002/chin.v36:3310.1002/chin.200533055.
[28] N. Jiang, A.J. Ragauskas, TEMPO-catalyzed oxidation of benzylic alcohols to aldehydes with the H_2O_2/HBr/ionic liquid [bmim]PF_6 system, Tetrahedron Lett. 46 (19) (2005) 3323–3326.
[29] S.J. Ha, E.-Y. Jung, W.M. Kim, J.C. Lee, Oxidation of Benzylic Alcohols with Urea Hydrogen Peroxide/Calcium Chloride in PEGDME 250, Bull. Korean Chem. Soc. 35 (2) (2014) 629–630.
[30] H. Park, J. Lee, Oxidation of benzylic alcohols with urea-hydrogen peroxide and catalytic magnesium bromide, Synlett 2009 (01) (2009) 79–80.
[31] H. Kargar, Synthesis, characterization and crystal structure of a manganese (III) Schiff base complex and investigation of its catalytic activity in the oxidation of benzylic alcohols, Transition Met. Chem. 39 (7) (2014) 811–817.
[32] X-AREA, version 1.30, program for the acquisition and analysis of data, Stoe & Cie GmbH, Darmstadt, Germany, (2005).
[33] X-RED, version 1.28b, program for data reduction and absorption correction, Stoe & Cie GmbH, Darmstadt, Germany, (2005).
[34] X-SHAPE, version 2.05, program for crystal optimization for numerical absorption correction, Stoe & Cie GmbH, Darmstadt, Germany, (2004).
[35] M.C. Burla, R. Caliandro, M. Camalli, B. Carrozzini, G.L. Cascarano, L. De Caro, C. Giacovazzo, G. Polidori, R. Spagna, SIR2004: an improved tool for crystal structure determination and refinement, J. Appl. Crystallogr. 38 (2005) 381–388.
[36] G.M. Sheldrick, A short history of SHELX, Acta Crystallogr, A 64 (2008) 112–122.
[37] M.J. Frisch, G.W. Trucks, H.B. Schlegel, G.E. Scuseria, M.A. Robb, J.R. Cheeseman, G. Scalmani, V. Barone, B. Mennucci, G.A. Petersson, H. Nakatsuji, M. Caricato, X. Li, H.P. Hratchian, A.F. Izmaylov, J. Bloino, G. Zheng, J.L. Sonnenberg, M. Hada, M. Ehara, K. Toyota, R. Fukuda, J. Hasegawa, M. Ishida, T. Nakajima, Y. Honda, O. Kitao, H. Nakai, T. Vreven, J.A. Montgomery, Jr., J.E. Peralta, F. Ogliaro, M. Bearpark, J.J. Heyd, E. Brothers, K.N. Kudin, V.N. Staroverov, T. Keith, R. Kobayashi, J. Normand, K. Raghavachari, A. Rendell, J.C. Burant, S.S. Iyengar, J. Tomasi, M. Cossi, N. Rega, J.M. Millam, M. Klene, J.E. Knox, J.B. Cross, V. Bakken, C. Adamo, J. Jaramillo, R. Gomperts, R.E. Stratmann, O. Yazyev, A.J. Austin, R. Cammi, C. Pomelli, J.W. Ochterski, R.L. Martin, K. Morokuma, V.G. Zakrzewski, G.A. Voth, P. Salvador, J.J. Dannenberg, S. Dapprich, A.D. Daniels, O. Farkas, J.B. Foresman, J.V. Ortiz, J. Cioslowski, D.J. Fox, GAUSSIAN 09 (Revision D.01), Gaussian, Inc., Wallingford, CT (2013).
[38] A.D. Becke, Density-functional thermochemistry. III. The role of exact exchange, J. Chem. Phys. 98 (7) (1993) 5648–5652.
[39] J. Tomasi, B. Mennucci, R. Cammi, Quantum mechanical continuum solvation models, Chem. Rev. 105 (8) (2005) 2999–3094.
[40] F. Weigend, R. Ahlrichs, Balanced basis sets of split valence, triple zeta valence and quadruple zeta valence quality for H to Rn: Design and assessment of accuracy, Phys. Chem. Chem. Phys. 7 (18) (2005) 3297, https://doi.org/10.1039/b508541a.
[41] J. Gauss, Effects of electron correlation in the calculation of nuclear magnetic resonance chemical shifts, J. Chem. Phys. 99 (5) (1993) 3629–3643.
[42] J.R. Cheeseman, G.W. Trucks, T.A. Keith, M.J. Frisch, " Comparison of models for calculating nuclear magnetic resonance shielding tensors, J. Chem. Phys. 104 (1996) 5497–5509.
[43] K. Wolinski, J.F. Hinton, P. Pulay, Efficient implementation of the Gauge-independent atomic orbital method for NMR chemical shift calculations, J. Am. Chem. Soc. 112 (23) (1990) 8251–8260.
[44] http://www.chemissian.com
[45] P. Sivajeyanthi, B. Edison, K. Balasubramani, G. Premkumar, T. Swu, Crystal structure, Hirshfeld surface analysis and HOMO–LUMO analysis of (E)-N′-(3-hydroxy-4-methoxybenzylidene)nicotinohydrazide monohydrate, Acta Crystallogr. E 75 (6) (2019) 804–807.
[46] W.X. Xu, W.H. Li, Synthesis, crystal structures, and catalytic property of dioxomolybdenum(VI) complexes with hydrazones, Russ. J. Coord. Chem. 38 (2) (2012) 92–98.
[47] V. Vrdoljak, B. Prugovecki, D. Matkovic-Calogovi, J. Pisk, R. Dreos, P. Siega, Supramolecular hexagon and chain coordination polymer containing the MoO_2^{2+} core: Structural transformation in the solid state, Cryst. Growth Des. 11 (2011) 1244–1252.
[48] M.R. Maurya, S. Agarwal, C. Bader, M. Ebel, D. Rehder, Synthesis, characterisation and catalytic potential of hydrazonato-vanadium(V) model complexes with $[VO]^{3+}$ and $[VO_2]^+$ cores, Dalton Trans. (3) (2005) 537, https://doi.org/10.1039/b416292g.

[49] S.D. Kurbah, M. Asthana, I. Syiemlieh, A.A. Lywait, M. Longchar, R.A. Lal, New dioxido-vanadium(V) complexes containing hydrazone ligands: Syntheses, crystal structure and their catalytic application toward C-H bond functionalization, J. Organomet. Chem. 876 (2018) 10–16.
[50] M. Ashfaq, A. Ali, A. Kuznetsov, M.N. Tahir, M. Khalid, DFT and single-crystal investigation of the pyrimethamine-based novel co-crystal salt: 2,4-diamino-5-(4-chlorophenyl)-6-ethylpyrimidin-1-ium-4-methylbenzoate hydrate (1:1:1)(DEMH), J. Mol. Struct. 1228 (2020) 129445.
[51] K.S. Munawar, S. Ali, M.N. Tahir, N. Khalid, Q. Abbas, I.Z. Qureshi, M. Ashfaq, Synthesis, spectroscopic characterization, X-ray crystal structure, antimicrobial, DNA-binding, alkaline phosphatase and insulin-mimetic studies of oxidovanadium (IV) complexes of azomethine precursors, J. Coord. Chem. 73 (2020) 2275–2300.
[52] S. Gao, X.-F. Zhang, L.-H. Huo, H. Zhao, (Methanol-κO)[3-methoxysalicylaldehyde (4-methoxybenzoyl)hydrazonato(2−)-κ^3O, O′, N]dioxomolybdenum(VI), Acta Crystallogr, E 60 (11) (2004) m1731–m1733.
[53] A. Rana, R. Dinda, P. Sengupta, S. Ghosh, L.R. Falvello, Synthesis, characterisation and crystal structure of cis-dioxomolybdenum(VI) complexes of some potentially pentadentate but functionally tridentate (ONS) donor ligands, Polyhedron 21 (2002) 1023–1030.
[54] V. Vrdoljak, M. Cindric, D. Milic, D. Matkovic-Calogovic, P. Novak, B. Kamenar, Synthesis of five new molybdenum(VI) thiosemicarbazonato complexes. Crystal structures of salicylaldehyde and 3-methoxy-salicylaldehyde 4-methylthiosemicarbazones and their molybdenum(VI) complexes, Polyhedron 24 (2005) 1717–1726.
[55] N.K. Ngan, K.M. Lo, C.S.R. Wong, Synthesis, structure studies and electrochemistry of molybdenum(VI) Schiff base complexes in the presence of different donor solvent molecules, Polyhedron 30 (17) (2011) 2922–2932.
[56] G. Romanowski, J. Kira, M. Wera, Five- and six-coordinate vanadium(V) complexes with tridentate Schiff base ligands derived from S(+)-isoleucinol: Synthesis, characterization and catalytic activity in the oxidation of sulfides and olefins, Polyhedron 67 (2014) 529–539.
[57] M. Karman, M. Wera, G. Romanowski, Chiral cis-dioxidomolybdenum(VI) complexes with Schiff bases possessing two alkoxide groups: Synthesis, structure, spectroscopic studies and their catalytic activity in sulfoxidation and epoxidation, Polyhedron 187 (2020) 114653.